American Mineralogist, Volume 81, pages 822–832, 1996

High-temperature structural study of germanate perovskites and pyroxenoids

D. ANDRAULT,[1] J.-P. ITIÉ,[2] AND F. FARGES[3]

[1]Département des Géomatériaux IPGP, URA CNRS 734, Université Paris 7, 4 place Jussieu, 75252 Paris, France
[2]Laboratoire de Physique de la Matière condensée, Université Paris 6, 4 place Jussieu, 75252 Paris, France
[3]Université Marne-la-vallée, URA CNRS 734, 2 allée de la butte verte, 93166 Noisy-le-grand, France

ABSTRACT

The $CaGeO_3$ and $SrGeO_3$ perovskites and $CaGeO_3$, $SrGeO_3$, and $MnGeO_3$ pyroxenoids have been studied at high-temperature by X-ray diffraction (XRD) and X-ray absorption fine-structure spectroscopy (XAFS). The diffraction studies show that the back-transformation of the perovskite begins at lower temperature for $SrGeO_3$ (~500 K) than $CaGeO_3$ (~945 K). An intensity reduction of the Bragg lines and the presence of a diffuse band in the diffraction patterns show the occurrence of transient amorphous phases. This transient phase contains Ge in fourfold and sixfold coordination after the loss of $CaGeO_3$ and $SrGeO_3$ perovskites, respectively. The recrystallization of the stable pyroxenoids occurs at higher temperature in a second step of the transformation.

For these compounds, the anharmonic character of the first Ge-O bond was extracted from the XAFS analysis. For the perovskites, we observed that the bulk thermal expansion and the Ge-O bond anharmonicity are closely connected. Both parameters are higher for cubic $SrGeO_3$ and simultaneously increase near 525 K when $CaGeO_3$ changes symmetry. For the pyroxenoids, our calculated tetrahedral thermal expansion is lower than for the bulk, with Ge-O bond anharmonicity very low. Close to the melting point, anomalous motion of the tetrahedral chains is suggested by a significant increase of the Ge-O bond length.

INTRODUCTION

Coordination changes around cations in minerals are of great interest in geophysics. The motivation for their study is related to the transition zone of the Earth, lying between 400 and 670 km depth. In this zone, Si is thought to modify its coordination number with O from four to six. Along with this transformation, denser mineral assemblages are probably formed, producing the seismic discontinuity between the upper and lower mantle (Ringwood 1991). The chemical connection between the two reservoirs of the mantle is not yet clearly understood, but it is generally accepted that there is some exchange of material. The mechanism of the phase transformations involved during this exchange is the main object of this study. The high-density structure studied is perovskite, the high-pressure form of pyroxenoid, which is stable under standard conditions.

In the Earth's mantle, the P-T phase diagram of $MgSiO_3$ pyroxene, garnet, and perovskite has been extensively discussed, and the stability fields for each structure have been checked using measured thermodynamic parameters (see Gasparik 1990; Yusa et al. 1993). The kinetics of these transformations are much less understood, but this discussion is of importance only for laboratory experiments because the geological time scale favors complete thermodynamic equilibrium. Nevertheless, experimental studies have shown that the mechanisms of phase transformation are complex and that important phenomena occur that could be of geophysical importance. For example, transient phases have been observed during the high-pressure transformations of forsterite and quartz, phases that could occur in geological conditions as transition layers (Guyot et al. 1990; Brearley et al. 1992; Winters et al. 1992). The physical properties of these transient phases, often poorly ordered, are unknown.

The experimental study of phase transformations involving changes in Si coordination is difficult. The quantity of material that can be loaded under extreme pressures and temperatures is limited. Also, the high-pressure experimental setup restricts the number of in situ techniques that can be used to investigate the sample. Thus, the same phase transformations must be reproduced under simpler conditions. This can be accomplished using analogs like germanates, which undergo comparable phase transformations but at lower pressure conditions (Ringwood and Seabrook 1963; Ross et al. 1986). For example, $CaGeO_3$, a close analog of $MgSiO_3$ perovskite, can be synthesized above 7 instead of 23 GPa. The germanate high-pressure compounds are more stable, and their properties can be more easily studied as a function of temperature or pressure. Furthermore, Ge analogs can be studied by X-ray absorption, which gives information on the local structure of Ge during phase transformations (Itié 1992; Andrault et al. 1992).

The cation-coordination change can also be studied during the back-transformation. At room pressure, high-

0003–004X/96/0708–0822$05.00

pressure metastable structures undergo a phase transformation to room-pressure polymorphs with heating. Previous studies have discussed the back-transformation in various perovskites. For the $MgSiO_3$ composition, the stability of the quenched high-pressure phase is reduced (see Knittle and Jeanloz 1987), and its structure can be observed only with careful electron microscopy (Wang et al. 1992). The stability of cubic $CaSiO_3$ perovskite is even lower, and this material spontaneously amorphizes after pressure quench (Wang and Weidner 1994). In the case of germanate perovskites, the stability is much higher, and thermal expansion can be studied up to several hundred degrees. $CaGeO_3$ perovskite changes its symmetry from orthorhombic to tetragonal at 525 K (Liu et al. 1991). Then, it back-transforms above 930 K, producing an amorphous phase (Durben et al. 1991). The reason for the formation of this transient amorphous phase, and the possible analogy with other perovskite compositions, must be studied more extensively to understand better the mechanism of the back-transformation.

Experiments

Samples

The germanate compositions $CaGeO_3$, $SrGeO_3$, and $MnGeO_3$ were studied, having the wollastonite, pseudowollastonite, and orthopyroxene structures, respectively, under ambient conditions. These pyroxenoid samples were finely ground in an agate mortar and then loaded into a high-temperature cell. Melting temperatures (Levin and McMurdie 1975) of 1693, 1713, and 1563 K for the $CaGeO_3$, $SrGeO_3$, and $MnGeO_3$ pyroxenoids, respectively, were reached in our experiments. For the Ca and Sr compositions, we also used the related metastable perovskites, previously synthesized at high pressure in large-volume apparatus. The orthorhombic $CaGeO_3$ perovskite (*Pbnm*) was synthesized by F. Guyot in a uniaxial split-sphere apparatus (USSA 2000) at the Center for High Pressure Research at the State University of New York at Stony Brook. The cubic $SrGeO_3$ perovskite (*Pm3m*) was synthesized by N.L. Ross at the Department of Geological Sciences, University College London. The perovskite samples were broken into chips about 100 μm in size to avoid formation of pyroxenoid during grinding. The purity of these perovskites is high, and all X-ray diffraction (XRD) lines could be correctly indexed (see Shimizu et al. 1970; Sasaki et al. 1983). The mean interatomic Ge-O bond lengths of these five compounds are compiled in Table 1.

Table 1. Mean first interatomic Ge-O bond length

Sample	$r_{Ge\text{-}O}$ (Å)	Method	Ref.
		Perovskites	
$CaGeO_3$	1.892	Diffraction	Sasaki et al. (1983)
$SrGeO_3$	1.898	Diffraction	Shimizu et al. (1970)
		Pyroxenoids	
$CaGeO_3$	1.76	Estimated	see Andrault et al. (1992)
$SrGeO_3$	1.80	Diffraction	Himler (1963)
$MnGeO_3$	1.756	Diffraction	Fang and Townes (1969)

Heating-wire technique

The samples were loaded into a 400 μm hole drilled into the flattened end of a 1 mm diameter platinum wire, as described in detail by Richet et al. (1993). This wire, about 70 mm long, was heated by the Joule effect up to the melting point of the germanates. The high-temperature cell allows temperature changes to be made in <3 min. The temperature measurement relies on a calibration of the electrical power, which was performed prior to the experiments and used various salts and minerals with known melting points. The precision is ±25 K at 1800 K. The temperature variation between the center of the sample and the border of the hole is about 10 K. The temperature reproducibility between the XAFS and X-ray diffraction experiments is about 25 K because the experiments were not performed with the same heating wires or at the same time. The acquisition times of the X-ray diffraction and XAFS experiments were different (20 min and 20 s, respectively), and thus the kinetics of transformation could be different for the two experimental setups.

X-ray diffraction

The X-ray diffraction patterns were recorded using an energy-dispersive configuration on the wiggler line of the DCI storage ring of LURE (Orsay). The polychromatic X-ray beam was collimated using tungsten carbide slits to 200 μm height and 50 μm width. The diffracted X-rays were collected with a Canberra planar germanium detector with a 2θ angle of ~14° for energies between 5 and 60 keV. The data-collection time ranged from ~15 to 30 min for the perovskites and pyroxenoids, respectively. From the diffraction patterns, the central position and the line width for each reflection were refined using a deconvolution program. For $SrGeO_3$ and $CaGeO_3$ perovskites, the unit-cell refinements were made with the assumption of cubic or pseudocubic symmetry.

The X-ray diffraction spectra represent the sum of the Bragg contribution generated by each crystalline phase present in the sample. We were able to calculate the perovskite unit-cell volumes during the back-transformation, even if the remaining fraction was very small. In contrast, the X-ray absorption signal recorded in transmission mode is related to the weighted addition of the different phases in the entire sample. X-ray absorption fine-structure (XAFS) results are thus preferentially characteristic of the dominant phase, crystalline or amorphous. The two techniques are complementary if the major phase is amorphous and if each method gives information on a different fraction of material.

X-ray absorption fine-structure spectroscopy

XAFS spectra at the Ge *K* edge were recorded at the DCI storage ring of LURE using the energy-dispersive configuration. A bent ellipsoidal Si(111) crystal was used

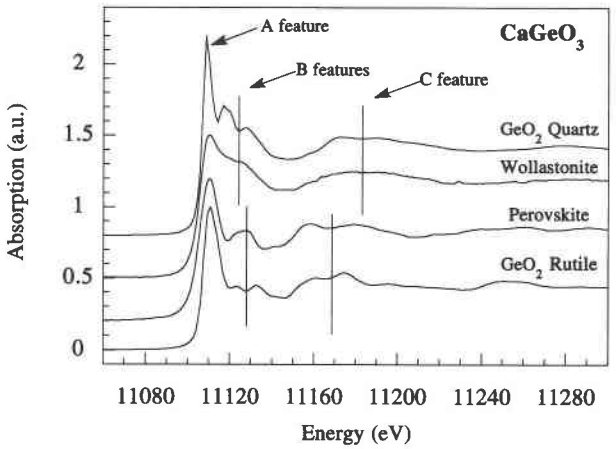

FIGURE 1. Ge *K*-edge absorption spectra of germanate compounds with Ge in fourfold or sixfold coordination.

to focus the polychromatic X-ray beam through the 400 μm wide sample. An array of 1024 photodiodes allowed spectrum acquisition times ranging from 1 to 30 s (see Dartyge et al. 1986). The absorption spectrum of metallic germanium was used to calibrate the photodiodes as a function of energy. For our experimental spectra usable energies ranged from 11050 to 11650 eV. The Ge absorption edges in $CaGeO_3$ wollastonite and perovskite are shown in Figure 1 in comparison with those of GeO_2 quartz and rutile recorded using a classical monochromator scan (courtesy of F. Vannereau). This figure shows clearly that the X-ray absorption near-edge structure (XANES) changes significantly when the local structure around Ge changes. The feature C is strongly related to the first maximum of the Ge-O XAFS oscillation. A shift toward low energies qualitatively corresponds to an increase of the Ge-O bond length (see Teo 1986). The nature of the A and B features is more complex, but these features are related to the site geometry of the absorbing element, including size and distortion. As described in previous studies (see Okuno et al. 1986), the energy of their centers and the intensity of the B feature are significantly different when Ge is located in tetrahedra or octahedra.

The spectra were normalized using a spline function and assuming an E_0 energy value located at the one-half height of the absorption step. After a k^3 Fourier transformation, the first XAFS contribution corresponding to the first Ge-O shell was isolated and Fourier back-transformed. For the theoretical modeling of each set of experiments, the room-temperature spectrum was used as a reference for the results at higher temperature. Initially we used the classical XAFS harmonic expression, where $\chi(k)$ is expressed in k space as follows (see Teo 1986):

$$\chi(k) = \sum_j A_j(k) \sin[2kr_j + \phi_{ij}(k)]. \quad (1)$$

The sinusoidal wave, corresponding to the N_j neighbors at distance r_j from the absorbing atom, is characterized by a phase shift, $\phi_{ij}(k)$, and an amplitude, A_j, given by

$$A_j = \frac{N_j S_i(k) F_j(k) \exp(-2\sigma_j^2 k^2) \exp[-2r_j/\lambda_j(k)]}{kr_j^2} \quad (2)$$

where $S_i(k)$ is an amplitude reduction factor, $F_j(k)$ is the backscattering amplitude from each of the N_j neighbors at distance r_j, with a Debye-Waller factor, σ_j, taking into account static disorder and vibrations along the bond direction; the term in $\exp(-2r_j/\lambda_j)$ is due to inelastic losses, with λ_j being the mean free path of electrons. Thus, the modeling gives quantitative information on the variation of Ge-O bond length, $r_{Ge\text{-}O}$, and disorder parameter, σ_j ($\sigma_j^2 = \sigma_{static}^2 + \sigma_{vibrational}^2$), as a function of temperature. The $\Delta\sigma^2$ notation used below indicates the relative departure of the square of σ_j from the room-temperature value.

When the partial radial distribution function, $g(r)$, departs from Gaussian shape, Equation 1 is no longer adequate to represent experimental results. Indeed, when the interatomic bond anharmonicity increases, $g(r)$ asymmetrically extends its contribution to higher $r_{Ge\text{-}O}$ values. The modeling of this shape with the use of a Gaussian function poorly reproduces the asymmetrical parts and yields a value of $r_{Ge\text{-}O}$ lower than the mean bond length. We thus used the cumulant expansion method, where $g(r)$ is expressed as the sum of cumulant C_n of increasing order. Introducing the cumulants in Equation 1 results in an additional multiplicative amplitude term, δA, and an additional phase-shift correction term, $\delta\phi$. The relationship between these two terms and the C_n expression developed to the fourth order is as follows (Crozier et al. 1988; Stern et al. 1991):

$$\delta\phi = -\frac{4}{3} C_3 k^3$$

$$\delta A = \exp\left(\frac{2}{3} C_4 k^4\right). \quad (3)$$

On the basis of these expressions, the third-order parameter (C_3) was used to define the departure of the interatomic potential from harmonicity because the fourth-order parameter (C_4) is usually found to be negligible. More information on C_3 measurement in the heating cell can be found in Farges et al. (1995). The ΔC_3 notation used below indicates the relative departure of C_3 from the room-temperature value. During the heating, the relative errors were estimated to within ± 0.005 Å for the interatomic bond length ($r_{Ge\text{-}O}$), $\pm 3 \times 10^{-4}$ Å^2 for the disorder factor ($\Delta\sigma^2$), and $\pm 10^{-4}$ Å^3 for the anharmonic parameter (ΔC_3).

THERMAL EXPANSION

Perovskites

Up to ten peaks were extracted from the diffraction patterns of $CaGeO_3$ perovskite, with d_{hkl} ranging from 3.72 to 1.05 Å. Most of these Bragg lines correspond to the pseudocubic unit cell that approximates this orthorhombic compound. The diffraction peaks related to the orthorhombic form of $CaGeO_3$ are poorly defined and cannot be continuously followed with increasing temper-

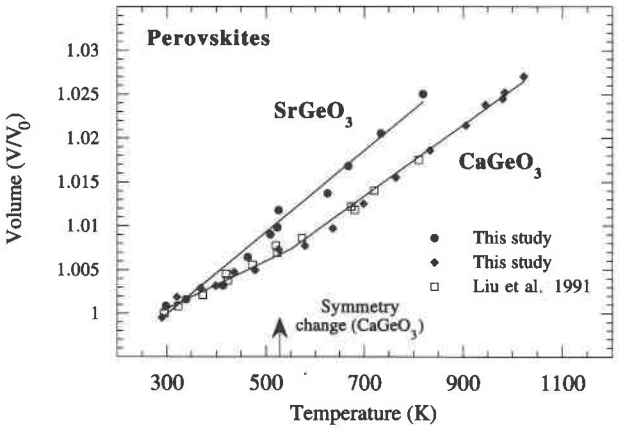

FIGURE 2. Temperature evolution of the unit-cell volume of $CaGeO_3$ and $SrGeO_3$ perovskites derived from X-ray diffraction results. Estimated volume errors are <2‰.

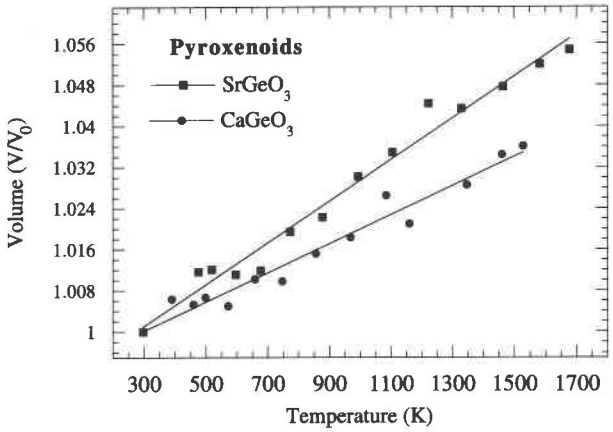

FIGURE 3. Temperature evolution of the volume of triclinic $CaGeO_3$ wollastonite and hexagonal $SrGeO_3$ pseudowollastonite. Estimated volume errors are within 3 and 2‰ for $CaGeO_3$ and $SrGeO_3$, respectively.

ature. Thus, at all temperatures eight diffraction lines were used for the pseudocubic unit-cell refinements. At higher temperature, the perovskite Bragg line intensities decrease because the metastable structure disappears above 930 K (see Durben et al. 1991). However, the perovskite lines remained sufficiently intense to allow for unit-cell volume refinements up to 1020 K (Fig. 2). The precision of the unit-cell volume determination is lower than 2‰. Our results are not precise enough to give new insight about possible slight structural modifications in $CaGeO_3$ perovskite. Indeed, the results of Liu et al. (1991) suggested that there is a symmetry change to the *Cmcm* space group at 525 K. With the assumption that this symmetry change occurs, volume thermal expansion values of 31(1) $\times 10^{-6}$ and 40(2) $\times 10^{-6}$ K^{-1} below and above 525 K, respectively, were calculated using both sets of data.

Similar spectra were collected for $SrGeO_3$ perovskite, and up to ten diffraction peaks were used for refinement of the volume of the cubic unit cell, with errors lower than 2‰. We observed that the intensity of the perovskite Bragg lines decreased progressively above 525 K. This decreased the quality of the refinements, but unit-cell volumes were derived using three remaining lines up to 850 K. The results are shown in Figure 2, where the calculated volume thermal expansion is 46(2) $\times 10^{-6}$ K^{-1}.

Pyroxenoids

For $CaGeO_3$ wollastonite, nine intense peaks with d_{hkl} between 4.8 and 2.7 Å were followed up to the melting point and used for the triclinic unit-cell refinements. Estimated precisions of the volumes are better than 3‰. Results are presented in Figure 3, where thermal expansion appears constant with temperature with a value of 28(2) $\times 10^{-6}$ K^{-1}. The *a*-axis linear expansion appears to be greater, with the *b* and *c* axes nearly unchanged with increasing temperature. Calculated values are 14(1) $\times 10^{-6}$, 5.1(1.0) $\times 10^{-6}$, and 2.4(0.5) $\times 10^{-6}$ K^{-1} for the three axes, respectively. Also, a slight decrease of the α angle between the *b* and *c* axes was observed with increasing temperature.

Similar results were obtained for $SrGeO_3$ pseudowollastonite up to the melting point. Nine peaks corresponding to d_{hkl} from 3.4 to 1.5 Å were used for the hexagonal refinements, with volume precision of better than 2‰ (Fig. 3). The volume thermal expansion appears constant with temperature to a value of 40(2) $\times 10^{-6}$ K^{-1}. The linear expansion of the *a* axis is slightly greater than that of the *c* axis, with values of 14.5(1.0) $\times 10^{-6}$ and 10.5(1.0) $\times 10^{-6}$ K^{-1}, respectively. No particular changes in the expansion curve were observed up the melting point. For both $CaGeO_3$ and $SrGeO_3$, the thermal expansion of pyroxenoids appears to be about 10% lower than that of the corresponding perovskites (see Table 2).

OCTAHEDRAL-TO-TETRAHEDRAL TRANSFORMATION

Back-transformation: X-ray diffraction results

The high-temperature evolution of the diffraction patterns of $CaGeO_3$ perovskite is shown in Figure 4. Ge fluorescence lines were used to normalize intensities. The diffraction peak intensities decreased above 945 K. This is related to the progressive loss of the perovskite with the gain of another polymorph of $CaGeO_3$. At temperatures between 945 and 1020 K, a clear diffuse band was observed near 20 keV, the energy that corresponds to the bond-length value of 2.8 Å. This band is the first-order contribution to the X-ray diffraction pattern from the amorphous compound. Other contributions were not observed because either their intensities were reduced or they were outside the energy range. It is thus impossible to get precise information about the amorphous structure through classical Fourier techniques. Nevertheless, the characteristic bond-length value of 2.8 Å should approximately correspond to O-O and Ca-O interatomic distances in the amorphous phase. This result confirms that a transient polymorph appears during back-transforma-

TABLE 2. Bulk and polyhedral thermal expansion of germanium perovskites and pyroxenoids

Sample	$\alpha(V)$ (K^{-1}, XRD)	$\alpha(GeO_x)$ (K^{-1}, XAFS)	Ref.
	Perovskites		
$CaGeO_3$	31×10^{-6} (below 525 K) 40×10^{-6} (up to 1020 K)		this study
$CaGeO_3$	31×10^{-6} (below 525 K) 35×10^{-6} (up to 810 K)		Liu et al. (1991)
$SrGeO_3$	46×10^{-6} (up to 850 K)		this study
	Pyroxenoids (up to melting points)		
$CaGeO_3$	28×10^{-6}	5.7×10^{-6}	this study
$SrGeO_3$	40×10^{-6}	5.7×10^{-6} (below 1250 K) 14×10^{-6} (above 1250 K)	this study this study
$MnGeO_3$		5.7×10^{-6}	this study

Note: The variable x is equal to six and four for perovskites and pyroxenoids, respectively.

tion, before recrystallization of wollastonite occurs at higher temperatures (Durben et al. 1991).

The case of $SrGeO_3$ perovskite is very similar to that of $CaGeO_3$. Clearly, the first step of the back-transformation leads to a noncrystalline phase. Above 525 K, the diffraction peaks of $SrGeO_3$ perovskite progressively disappear and vanish near 1080 K. For this compound, the amorphous diffuse band is less clear, but no major diffraction peaks were found in a large temperature range up to 1250 K. Characteristic diffraction spectra of pseudowollastonite were observed only at higher temperatures.

$CaGeO_3$ perovskite back-transformation: XAFS results

The temperature evolution of the X-ray absorption near-edge structure (XANES) of Ge in $CaGeO_3$ is presented in Figure 5a. The shapes of the spectra change above 945 K when the perovskite back-transforms, with significant modification of the energy position of the A, B, and C features. In relation to the previous description of Figure 1, these results suggest a change in Ge coordination number from six to four. For the spectra recorded at 1025 K, the A and B features appear less defined than those at higher temperature but clearly show Ge in fourfold coordination. This effect is due to higher disorder in

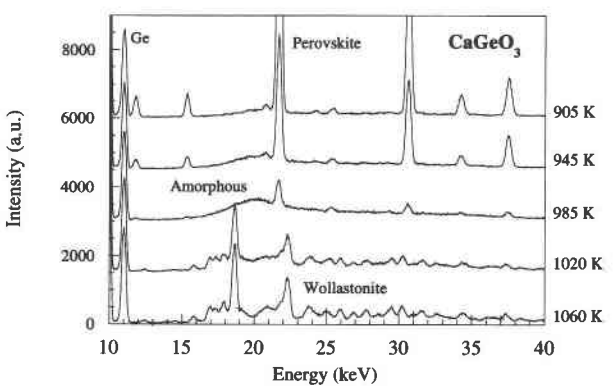

FIGURE 4. Diffraction spectra of $CaGeO_3$ during back-transformation of the perovskite.

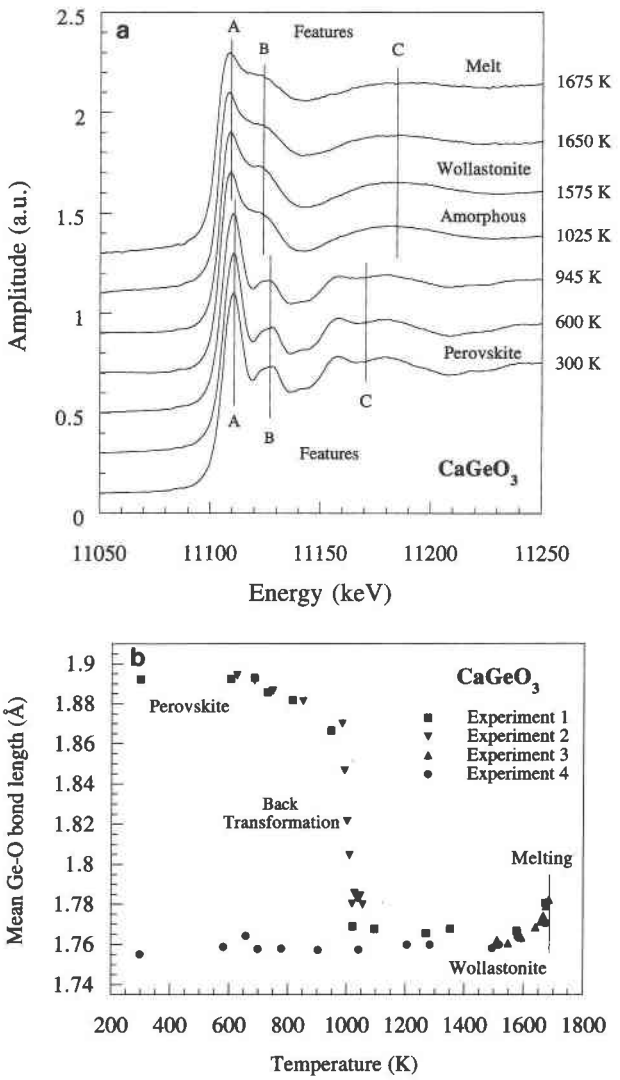

FIGURE 5. (a) Temperature evolution of the Ge *K*-edge absorption spectra in $CaGeO_3$ during back-transformation of the perovskite. The A, B, and C features are related to those described in Figure 1. (b) Mean Ge-O bond-length evolution estimated from XAFS harmonic model for a single O shell around Ge.

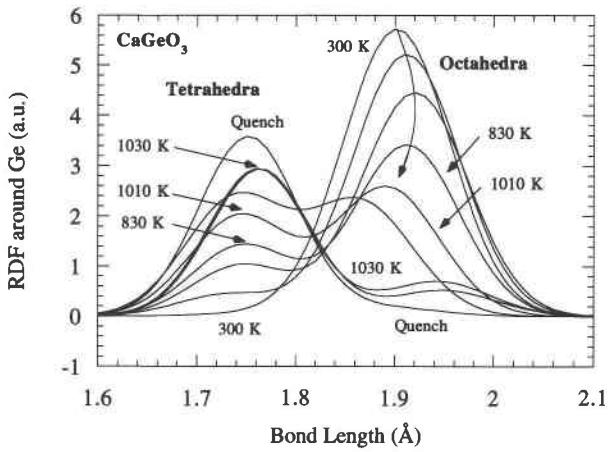

FIGURE 6. Temperature change of the partial radial distribution function around Ge. The slight increase of the tetrahedral contribution at low temperatures is an artifact of the calculation (see text).

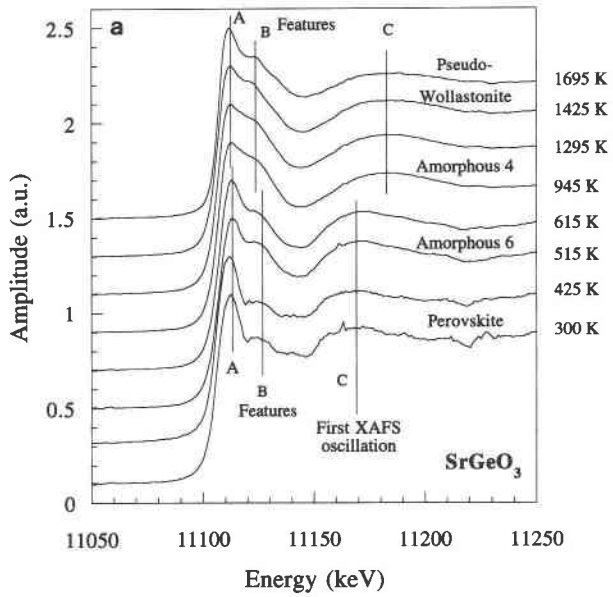

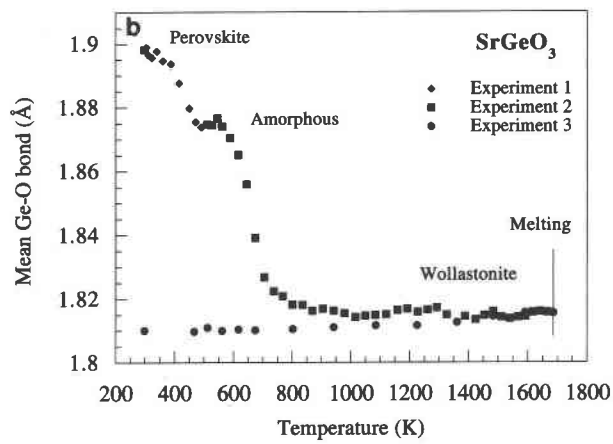

FIGURE 7. (a) Temperature evolution of the Ge *K*-edge absorption spectra in $SrGeO_3$ during back-transformation of the perovskite. The A, B, and C features are related to those described in Figure 1. (b) Mean Ge-O bond-length evolution estimated from XAFS harmonic model for a single O shell around Ge.

the local structure of Ge, and the 1025 K spectrum is related to the transient amorphous phase observed in the X-ray diffraction patterns. Also, the spectra recorded at 1675 K present a similar, poorly defined XANES that corresponds to the $CaGeO_3$ melt. Between 1025 and 1675 K, the spectra are of the wollastonite form.

From these absorption spectra recorded up to the melting points, the first Ge-O bond length was calculated using the classical Equation 1. Figure 5b shows that Ge-O bond length decreases during the back-transformation because of the Ge coordination change from octahedral to tetrahedral. The quality of the XAFS modeling of spectra recorded during the back-transformation is poor because the sample contains Ge in both fourfold and sixfold coordination. To model this transformation better, we also modeled the first XAFS contribution with two O shells, characterizing the two kinds of polyhedra coexisting in the sample. The principal adjustable parameters, therefore, were the proportions of Ge in fourfold or sixfold coordination. We used these XAFS parameters to recalculate the partial radial distribution function (RDF) around Ge. For that purpose, an arbitrary value of 0.05 $Å^2$ was chosen for the Ge-O disorder factor at ambient temperature. A Gaussian shape was calculated for each of the two shells using the refined parameters; the proportion of the respective shell, bond length, and disorder factor was corrected for ambient values. We then summed these two Gaussians, and selected results are presented in Figure 6 as a function of temperature. Again, the anomalous decrease of the octahedral Ge-O bond length owing to the increase of anharmonicity is noticeable. We also calculated a slight increase of the tetrahedral contribution at low temperature. This is not due to the appearance of Ge in tetrahedral sites below 945 K but to an improper attempt to model the increasing anharmonicity in the perovskite. In contrast, between 945 and 1020 K, the partial radial distribution functions contain a mix of two contributions, clearly illustrating the partial back-transformation of octahedra to tetrahedra. At higher temperature, the octahedral contribution becomes negligible in the RDF, which signals complete back-transformation.

$SrGeO_3$ perovskite back-transformation: XAFS results

XANES spectra of the Ge *K* edge in $SrGeO_3$ are presented in Figure 7a. As in the case of $CaGeO_3$, modifications of the shape with temperature are clear. The mean Ge-O bond length calculated with the harmonic Equation 1 is presented as a function of temperature in Figure 7b. The back-transformation is clearly followed by a Ge coordination change, which decreases the Ge-O bond length from ~1.898 to 1.80 Å, the expected values for perov-

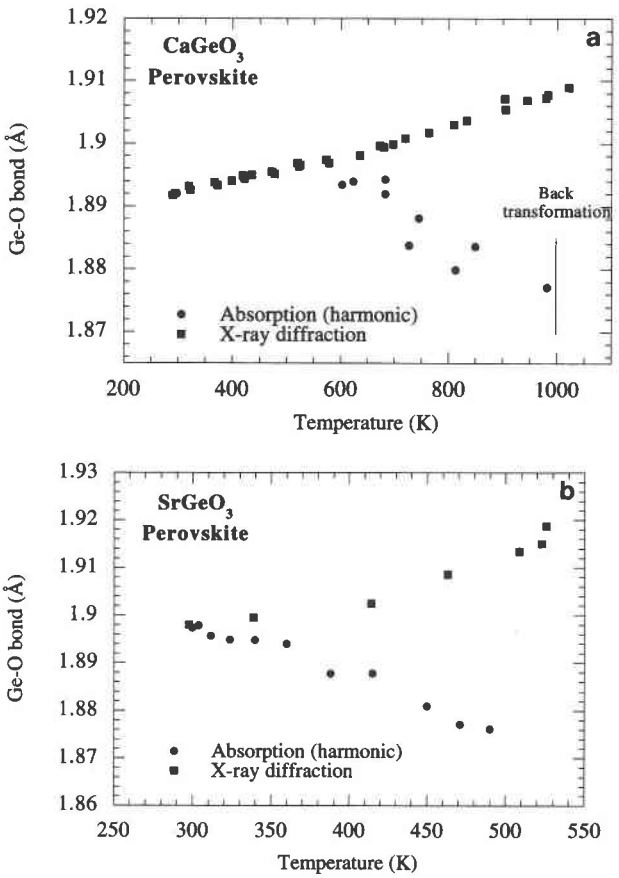

FIGURE 8. Temperature variation of the Ge-O bond length in (a) $CaGeO_3$ and (b) $SrGeO_3$ perovskites using a classical harmonic model. The discrepancy between the absorption and diffraction results is due to the increase of the Ge-O bond anharmonicity.

skite and pseudowollastonite, respectively. But unlike the $CaGeO_3$ results, the evolution presents an intermediate plateau for an r_{Ge-O} value of about 1.875 Å between 500 and 615 K. This feature suggests the formation of a transient phase with Ge in sixfold coordination. The shapes of the corresponding XANES spectra (Fig. 7a) vary slightly from the lower temperature spectrum, and the high similarity among the A, B, and C features suggests octahedral Ge. This effect, and the fact that X-ray diffraction spectra show no new lines in this temperature range, strongly suggests that an amorphous phase with octahedral Ge is formed during the back-transformation. Note that the occurrence of octahedral Ge is not surprising, considering that rutile is the stable polymorph of GeO_2 at the same temperature conditions.

The second step of the back-transformation occurs above 615 K. The shapes of the near-edge spectra as well as the calculated Ge-O bond length become characteristic of tetrahedral Ge coordination. Slight changes in the shape of the A and B features of spectra recorded between 900 and 1295 K imply that the fourfold-coordinated sample progressively recrystallizes. These results suggest that the back-transformation of $SrGeO_3$ involves changes from sixfold to fourfold coordination in the amorphous phases, in agreement with our X-ray diffraction results (Fig. 7a) showing no significant recrystallization below 1250 K.

It is interesting that the Ge-O bond length of about 1.81 Å for the fourfold-coordinated, amorphous transient phase is comparable to that in pseudowollastonite (1.80 Å). The same effect is also observed between the transient amorphous and wollastonite phases of $CaGeO_3$, but with a different Ge-O bond length of about 1.76 Å. According to a previous discussion of the variation of the Ge-O bond length in tetrahedra (Nishi and Takeuchi 1992), this observation suggests that the tetrahedral chains have very similar linkages in both the transient amorphous phase and related pyroxenoid.

POLYHEDRAL EXPANSION AND ANHARMONICITY

Ge-O bonds in perovskites

The low-temperature evolution of the Ge-O bond length in $CaGeO_3$ and $SrGeO_3$ perovskites is presented in Figure 8, which shows that the apparent Ge-O bond length decreases with increasing temperature. This behavior of the r_{Ge-O} XAFS parameter is not due to the decrease of the octahedral volume. The Ge-O bond length increases with temperature, and this increase is closely related to the volume thermal expansion. Indeed, because the octahedra have exactly (cubic) or approximately (orthorhombic) the same thermal expansion as the perovskite bulk, the octahedral volume expansion can be evaluated from the X-ray diffraction results (see Fig. 8). In fact, the anomalous behavior of r_{Ge-O} is characteristic of the increase of the Ge-O bond anharmonicity in the octahedra with increasing temperature. We thus reinvestigated the changes in octahedral XAFS parameters as a function of temperature with the anharmonic Equation 3. Also, to reduce the number of adjustable parameters for each temperature, we used the Ge-O bond length value calculated from the X-ray diffraction results.

The temperature evolution of the C_3 anharmonic parameter is presented in Figure 9a for both perovskites. As expected from the anomalous r_{Ge-O} evolution, C_3 increases with increasing temperature. This effect is more important for the $SrGeO_3$ than for the $CaGeO_3$ perovskite. For $CaGeO_3$ perovskite, the C_3 evolution shows a break below 600 K, with an increase of the Ge-O bond anharmonicity at higher temperature. This break could be related to the symmetry change observed for this perovskite at 525 K. Nevertheless, for the highest temperatures, the increase of C_3 with temperature in $CaGeO_3$ remains lower than for $SrGeO_3$. The temperatures of the onset of the perovskite back-transformations are reported in Figure 9a. For these particular temperatures, the relative variation of the C_3 anharmonic parameters is found to be about 170×10^{-5} Å^3 for both $CaGeO_3$ and $SrGeO_3$

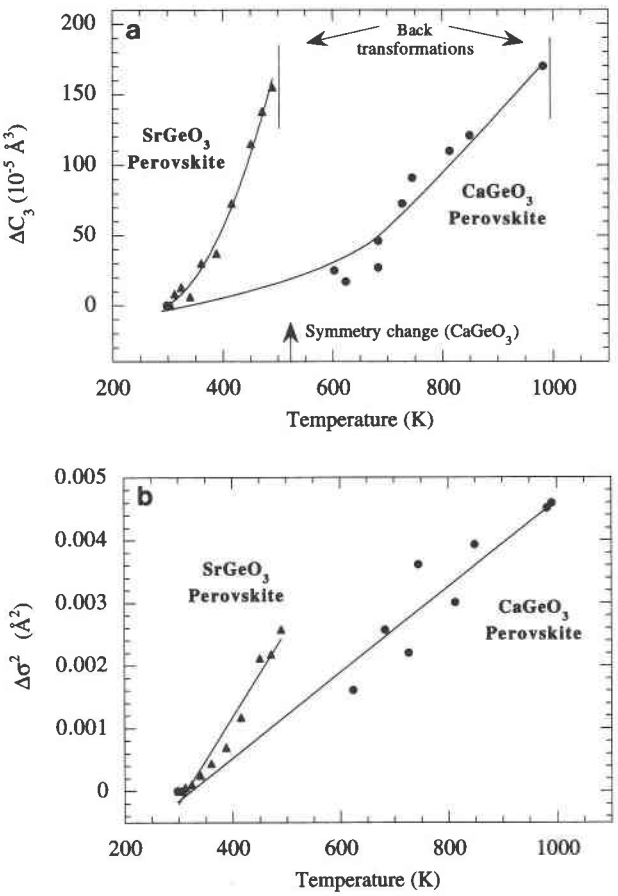

FIGURE 9. Temperature variation of the Ge-O bond (a) ΔC_3 anharmonic parameter and (b) $\Delta\sigma^2$ disorder parameter in $CaGeO_3$ and $SrGeO_3$ perovskites. For this calculation, bond-length values were estimated from X-ray diffraction results.

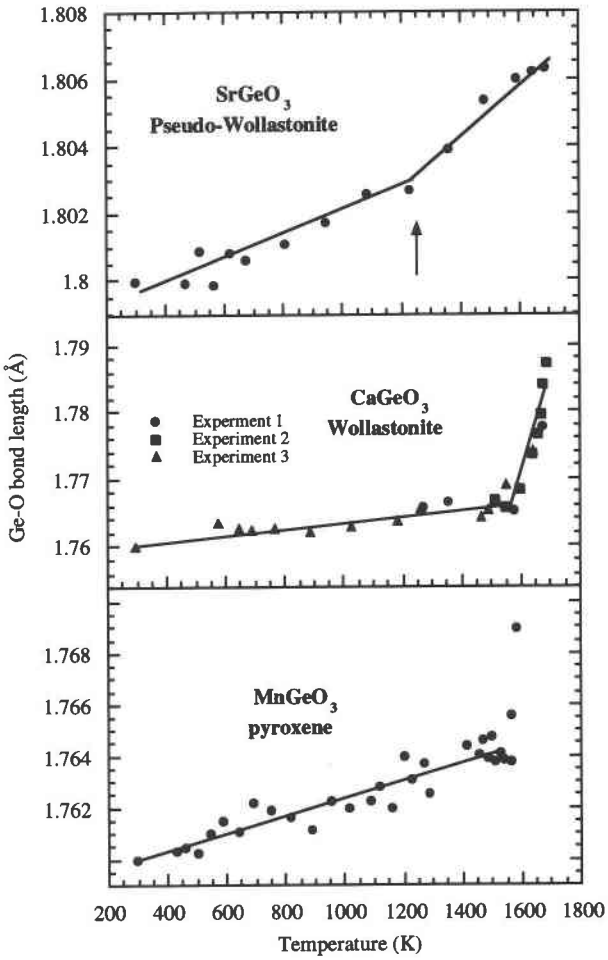

FIGURE 10. Temperature evolution of the Ge-O bond length in $SrGeO_3$, $CaGeO_3$, and $MnGeO_3$ pyroxenoids up to melting points, using an XAFS harmonic model.

perovskites. This means that both compounds have very similar Ge-O bond anharmonicity at temperatures just below the loss of the perovskite structure. The evolution of the $\Delta\sigma^2$ disorder factors is presented in Figure 9b, where the increase with temperature is larger for $SrGeO_3$ perovskite.

Ge-O bonds in pyroxenoids

The evolution of the first Ge-O bond length in pyroxenoids obtained from XAFS modeling using the harmonic Equation 1 is presented in Figure 10. The same set of experiments was also modeled with Equation 3, and only a slight increase of the C_3 anharmonic parameter was found. Both expressions produced very similar Ge-O bond-length values, and we thus choose Equation 1 to quantify our results. For the three compounds studied, the low-temperature tetrahedral volume thermal expansion is $5.7(5) \times 10^{-6}$ K^{-1}. This is lower than that for the whole structure (see Table 2), a result compatible with studies of other germanate or silicate structures (see Hazen and Finger 1982), showing that tetrahedral size is nearly constant during heating or compression. The calculated disorder factor, $\Delta\sigma^2$, also has a reduced variation of approximately 3×10^{-5} $Å^2$ between 300 and 1300 K.

For $SrGeO_3$ pseudowollastonite, the thermal evolution of the Ge-O bond length appears separated into two regimes, with tetrahedral thermal expansion of $14(1) \times 10^{-6}$ K^{-1} above about 1250 K. Also, we observed an anomalous increase of $r_{Ge\text{-}O}$ in $CaGeO_3$ and $MnGeO_3$ just below the melting temperature. For $CaGeO_3$, the tetrahedral volume thermal expansion is calculated to be $250(30) \times 10^{-6}$ K^{-1} between 1625 and 1690 K. This effect indicates important changes in the local structure around Ge just before melting. It cannot be explained by an increase of Ge-O bond anharmonicity in the tetrahedra, which would produce an anomalous decrease of the $r_{Ge\text{-}O}$ parameter. In the same temperature range, the shapes of the XANES absorption spectra (Fig. 5a) show a decrease of the defi-

TABLE 3. Thermal expansion of metastable $A^{2+}B^{4+}O_3$ perovskites compared with unit-cell volumes and molar mass

Sample	$\alpha(V)$ (K^{-1})	$V_{300\,K}$ ($Å^3$)	Mass (g)	Ref.
$MgSiO_3$	21×10^{-6}	40.70	100.40	Ross and Hazen (1989)
$CaSiO_3$	26×10^{-6}	45.83	116.16	Wang and Weidner (1994)
$CaGeO_3$	$31–40 \times 10^{-6}$	51.59	160.68	this study
$SrGeO_3$	46×10^{-6}	54.70	208.23	this study

Note: For $MgSiO_3$, the expansivity corresponds to the mean value between 300 and 500 K.

nition of the A and B features, strongly suggesting a decrease of the local order.

DISCUSSION

Thermal expansion of perovskite

An empirical law described by Hazen and Finger (1982) evaluates the bulk thermal expansion for a given polyhedron:

$$\alpha(K^{-1}) \approx 3 \times 4.0 \times 10^{-6}\left(\frac{n}{S^2 z_c z_a}\right). \quad (4)$$

In this expression, S^2 is an ionicity factor usually determined to be 0.50 for all oxides and silicates, z_c and z_a are the cation and anion valences, respectively, and n is the coordination number. Thermal expansion coefficients of $A^{2+}O_{12}^{2-}$ dodecahedra and $B^{4+}O_6^{2-}$ octahedra are estimated to be 72×10^{-6} and 18×10^{-6} K^{-1}, respectively, for all perovskites. For these polyhedra, because n, z_c, and z_a are defined, the volume thermal expansion of each unit should depend neither on the nature of the A cation nor on the size of the polyhedron. Thus, because perovskite is a close-packed structure formed with these two polyhedra, its volume thermal expansion should be very similar for all compositions. The only possible variation should be connected to changes of the octahedral orientation in distorted perovskites.

This property is not confirmed by experimental values of the bulk thermal expansion of metastable germanate and silicate perovskites (Table 3). Indeed, even for $CaSiO_3$ and $SrGeO_3$ cubic perovskites, significantly different bulk thermal expansions were found. For the four metastable compounds in Table 3, thermal expansion increases with unit-cell volume or with the molar mass under ambient conditions. This effect confirms that thermal expansion cannot be simply calculated from each polyhedral contribution and that dense structures exhibit much more complex unit-cell bonding (see Hemley and Cohen 1992).

Ge-O bond anharmonicity

The thermal expansion of a chosen polyhedron depends on the mechanism of the structural expansion, as extensively described by Hazen and Finger (1982). Our results illustrate this phenomenon quite well. Indeed, we observed a break in the tetrahedral thermal expansion in $SrGeO_3$ pseudowollastonite, a break not observed in the bulk thermal expansion curve. This shows that the mechanisms of thermal expansion affecting polyhedral expansion are slightly altered. In this study, we observed comparable effects for the temperature evolution of the C_3 anharmonic parameter. For GeO_6 octahedra, the anharmonicity of the Ge-O bond depends significantly on the composition. We measured a much higher Ge-O anharmonicity in $SrGeO_3$ than in $CaGeO_3$ perovskites. Also, the structural modification occurring at 525 K in $CaGeO_3$ perovskite induces a clear break in the anharmonic parameter evolution. These two effects, variable polyhedral expansion and Ge-O anharmonicity, are obviously closely related to each other. The simultaneous increase of both Ge-O anharmonicity and bulk thermal expansion in $CaGeO_3$ perovskite, and the high value of both thermal expansion and Ge-O anharmonicity in $SrGeO_3$ perovskite, confirm this.

Metastability

Another important observation is the strong increase of the Ge-O disorder factor in $SrGeO_3$ perovskite in comparison with that in $CaGeO_3$ perovskite (Fig. 9b). For cubic $SrGeO_3$ perovskite, because all Ge-O bonds are similar, this means an anomalous increase of the vibrational disorder. In this perovskite, octahedral expansion is identical to that of the unit cell, and the bulk thermal expansion (46×10^{-6} K^{-1}) is much higher than the octahedral expansion estimated from Equation 4 (18×10^{-6} K^{-1}). Thus, in $SrGeO_3$, the Ge-O bond lengths in octahedra become greater than a hypothetical value calculated with a thermal expansion of 18×10^{-6} K^{-1}. This contrasts with the $CaGeO_3$ orthorhombic perovskite, in which the octahedral volumes can be adjusted by variation of the tilt orientation to avoid such anomalously high Ge-O bond expansion. Experimental results illustrate this structural difference between the two compounds. At room temperature, the mean Ge-O bond length is already higher in $SrGeO_3$ (1.898 Å) than in $CaGeO_3$ (1.892 Å) perovskites. This difference increases with temperature from 3.2 to 4.7‰ at 300 and 800 K, respectively. This effect suggests that in $SrGeO_3$, the Ge is centered in the octahedron, where more important displacements are possible than in $CaGeO_3$. This particular structural behavior could explain the earlier back-transformation of the $SrGeO_3$ perovskite.

Our X-ray diffraction results are consistent with a previous Raman investigation (Durben et al. 1991) that suggested the formation of a transient amorphous phase during the back-transformation of $CaGeO_3$ perovskite. The same property was also observed for $SrGeO_3$ perovskite above about 500 K. This behavior and the fact that the stable pyroxenoids recrystallize only at higher temperature suggest that the loss of the perovskite structure is indeed due to intrinsic properties. The formation of transient phases during back-transformation seems to be

common because almost all high-pressure perovskites exhibit the same effect.

Anomalous premelting of pyroxenoids

For pyroxenoids, an anomalous increase of the Ge-O bond length was observed at temperatures just below melting. As mentioned above, this effect is due not only to an increase of the Ge-O anharmonicity in tetrahedra but also to unexpected changes in the local structure around Ge. Two hypotheses can explain these experimental observations: (1) Such anomalous behavior of tetrahedra could indicate premelting in the sample. Tetrahedral linkages within chains undergo unexpected change that causes the expansion mechanism of the structure to change. The interatomic bonding changes on a short time scale, without considerably changing the X-ray diffraction patterns (see Richet et al. 1996). This premelting effect could be related to an increase in the number of defects present in the structure before melting. (2) The anomalous increase of the Ge-O bond length could be related to partial melting already observed in other compounds (see Doukhan et al. 1993). A significant proportion of the sample could already have melted, even if the temperature remains below the melting point. With either hypothesis, to explain the increase of the Ge-O bond length the transformed phase must contain a significant amount of Ge-O with longer bond length than in the initial structure. This is possible if some octahedra have formed or if the transformed phase contains tetrahedra linked to each other in a different configuration. Indeed, as described by Nishi and Takeuchi (1992) the change in the Ge-O-Ge angles or in the covalence of the Ge-O bond can significantly affect the Ge-O bond length.

Acknowledgments

We thank P. Richet and A. Pierre for the high temperature cell facilities; F. Guyot and N.L. Ross for donating the $CaGeO_3$ and $SrGeO_3$ perovskite samples; F. Baudelet and E. Dartyge for their help during X-ray absorption measurements; P.-E. Petit, J.-P. Poirier, and P. Richet for a helpful review and fruitful comments. CNRS-INSU-DBT "Terre Profonde" contribution no. 47; IPGP contribution no. 1430.

References cited

Andrault, D., Madon, M., Itié, J.-P., and Fontaine, A. (1992) Compression and coordination changes in pyroxenoids: An EXAFS study of $MgGeO_3$ enstatite and $CaGeO_3$ wollastonite. Physics and Chemistry of Minerals, 18, 506–513.

Brearley, A.J., Rubie, D.C., and Ito, E. (1992) Mechanisms of the transformations between the α, β, and γ polymorphs of Mg_2SiO_4 at 15 GPa. Physics and Chemistry of Minerals, 18, 343–358.

Crozier, E.D., Rehr, J.J., and Ingalls, R. (1988) Amorphous and liquid systems. In D. Kroningsberger and R. Prins, Eds., X-ray absorption: Principles, applications, techniques of EXAFS, SEXAFS and XANES, p. 373–442. Wiley, New York.

Dartyge, E., Depautex, C., Dubuisson, J.M., Fontaine, A., Jucha, A., Leboucher, P., and Tourillon, G. (1986) X-ray absorption in dispersive mode, a new spectrometer and a data acquisition system for fast kinetics. Nuclear Instruments and Methods, A246, 452–460.

Doukhan, N., Doukhan, J.-C., Ingrin, J., Jaoul, O., and Raterron, P. (1993) Early partial melting in pyroxenes. American Mineralogist, 78, 1246–1256.

Durben, D.J., Wolf, G.H., and McMillan, P. (1991) Raman scattering study of the high temperature vibrational properties and stability of $CaGeO_3$ perovskite. Physics and Chemistry of Minerals, 18, 215–223.

Fang, J.H., and Townes, W.D. (1969) The crystal structure of manganese metagermanate $MnGeO_3$. Kristallographie, 130, 139–147.

Farges, F., Fiquet, G., Andrault, D., and Itié, J.-P. (1995) In situ high-temperature ($\rightarrow$ 2100 K) XAFS and anharmonicity. Physica B, 208 and 209, 263–264.

Gasparik, T. (1990) Phase relations in the transition zone. Journal of Geophysical Research, B95, 15751–15769.

Guyot, F., Gwanmesia, G.D., and Liebermann, R.C. (1990) An olivine to beta-phase transformation mechanism Mg_2SiO_4. Geophysical Research Letters, 18, 89–92.

Hazen, R.M., and Finger, L.W. (1982) Comparative crystal chemistry, 231 p. Wiley, New York.

Hemley, R.J., and Cohen, R.E. (1992) Silicate perovskite. Annual Review of Earth Planetary Sciences, 20, 553–600.

Himler, W. (1963) An X-ray investigation of the strontium germanate $SrGeO_3$. Soviet Physics—Crystallography, 7, 573–576.

Itié, J.-P. (1992) X-ray absorption spectroscopy under high pressure. Phase Transition, 39, 81–98.

Knittle, E., and Jeanloz, R. (1987) The activation energy of the back transformation of silicate perovskite to enstatite. In M. Manghnani and Y. Syono, Eds., High pressure in mineral physics, p. 243–250. Terra Scientific and American Geophysical Union, Washington, DC.

Levin, E.M., and McMurdie, H.F. (1975) Phase diagrams for ceramists. American Ceramic Society, Columbus, Ohio, p. 513.

Liu, X., Wang, Y., Liebermann, R.C., Maniar, P.D., and Navrotsky, A. (1991) Phase transition in $CaGeO_3$ perovskite: Evidence from X-ray powder diffraction, thermal expansion, and heat capacity. Physics and Chemistry of Minerals, 18, 224–230.

Nishi, F., and Takeuchi, Y. (1992) The nature and the variation of Ge-O bonding in germanates. Zeitschrift für Kristallographie, 202, 251–259.

Okuno, M., Yin, C.D., Morikawa, H., and Marumo, F. (1986) A high resolution EXAFS and near edge study of GeO_2 Glass. Journal of Non-Crystalline Solids, 87, 312–320.

Richet, P., Gillet, P., Pierre, A., Bouhifd, A., Daniel, I., and Fiquet, G. (1993) Raman spectroscopy, X-ray diffraction and phase relationship determinations with a versatile heating cell for measurements up to 3600 K (or 2700 K in air). Journal Applied Physics, 74, 5451–5456.

Richet, P., Mysen, B.O., and Andrault, D. (1996) Melting and premelting of silicates: Raman spectroscopy and X-ray diffraction of Li_2SiO_3 and Na_2SiO_3. Physics and Chemistry of Minerals, 22, in press.

Ringwood, A.E. (1991) Phase transformation and their bearing on the constitution and dynamics of the mantle. Geochimica et Cosmochimica Acta, 55, 2083–2110.

Ringwood, A.E., and Seabrook, M. (1963) High-pressure phase transformation in germanates pyroxenes and related compounds. Journal of Geophysical Research, 68, 4601–4609.

Ross, N.L., Akaogi, M., Navrotsky, A., Susaki, J., and McMillan, P. (1986) Phase transitions among $CaGeO_3$ polymorphs (wollastonite, garnet, and perovskite structures): Studies by high-pressure synthesis, high-temperature calorimetry and vibrational spectroscopy and calculation. Journal of Geophysical Research, 91, 4685–4696.

Ross, N.L., and Hazen, R.M. (1989) Single crystal X-ray diffraction study of $MgSiO_3$ perovskite from 77 to 400 K. Physics and Chemistry of Minerals, 46, 415–420.

Sasaki, S., Prewitt, C.T., and Liebermann, R.C. (1983) The crystal structure of $CaGeO_3$ perovskite and the crystal chemistry of $GdFeO_3$-type perovskites. American Mineralogist, 68, 1189–1198.

Shimizu, Y., Syono, Y., and Akimoto, S. (1970) High-pressure transformations in $SrGeO_3$, $SrSiO_3$, $BaGeO_3$, and $BaSiO_3$. High Temperature–High Pressure, 2, 113–120.

Stern, E.A., Livins, P., and Zhang, Z. (1991) Thermal vibration and melting from a local perspective. Physical Review, B43, 8850–8860.

Teo, B.K. (1986) EXAFS: Basics principles and data analysis, 349 p. Springer-Verlag, Berlin.

Wang, Y., Guyot, F., and Liebermann, R.C. (1992) Electron microscopy of $(Mg,Fe)SiO_3$: Evidence for structural phase transitions and implications for the lower mantle. Journal of Geophysical Research, 97, 12327–12347.

Wang, Y., and Weidner, D.J. (1994) Thermoelasticity of $CaSiO_3$ perovskite and implication for the lower mantle. Geophysical Research Letters, 21, 895–898.

Winters, R.R., Garg, A., and Hammack, W.S. (1992) High resolution transmission electron microscopy of pressure-amorphized α-quartz. Physical Review Letters, 69, 3751–3753.

Yusa, H., Akaogi, M., and Ito, E. (1993): Calorimetric study of $MgSiO_3$ garnet and pyroxene: Heat capacities, transition enthalpies, and equilibrium phase relations in $MgSiO_3$ at high pressures and temperatures. Journal of Geophysical Research, 98, 6453–6460.

Manuscript received September 25, 1995
Manuscript accepted March 4, 1996